The 2009 IEEE/RSJ International Conference on
Intelligent Robots and Systems
October 11-15, 2009 St. Louis, USA

Motion controller for the Atomic Force Microscopy based nanomanipulation system

Ruiguo Yang, Ning Xi, King Wai Chiu Lai, Bingtuan Gao, Hongzhi Chen, Chanmin Su and Jian Shi

Abstract—**Nanomanipulation with Atomic Force Microscopy (AFM) is one of the fundamental tools for nano-manufacturing. The control of the nanomanipulation system requires accurate feedback from the piezoelectric actuator and high frequency response of the control system. We designed and implemented two distinct control schemes by using real-time Linux. The aim is to study various factors in the control of the AFM based nanomanipulation system. By integrating the original controller with the external Linux real-time controller, we achieved a stable system with high response frequency. Finally this Multiple Input Single Output (MISO) system is validated to be an effective and efficient tool for the controlling of the nanolithography operation through a haptic device.**

I. INTRODUCTION

The atomic force microscopy (AFM) based nano-manipulation technique has been a quite useful tool in nano manufacturing as demonstrated by its abilty to perform nano lithography [1], assembly [2][3] and manipulating nano particles [4][5]. Besides, it holds the potential application in biological researches, like drug delivery and cell mechanics [6].

In [1], a nanometer pattern is created on a thin layer of polymer by manipulating the AFM tip to induce a current between the tip and the silicon substrate. The method is used to define a nanometer electrode by combining the AFM lithography and electron beam lithography. One of the main technique involved is the controlling of the AFM tip patterning. The assembly of nano structures has been achieved by [2]. In the nanoassembly process, not only nano particles has been manipulated, but also more complex structures like nano rode nanotube have been pushed by an AFM tip. This may eventually leads the way to the nanomanufacturing process. Manipulation of nanotubes has been of particular interest when bridging of two electrodes by carbon nanotubes (CNT) is considered. An AFM based nanomanipulation system is able to push the CNT onto electrodes and to make mechanical contact between the two. This makes the investigation of the characteristic property of CNT much more convenient [7].

This research work is partially supported under NSF grant IIS 0713346 and ONR Grants N00014-07-1-0935.

Ruiguo Yang, Ning Xi, King Wai Chiu Lai, Bingtuan Gao and Hongzhi Chen are with the Dept. of Electrical and Computer Engineering, Michigan State University, East Lansing, MI 48823 USA; yangruig@msu.edu.

Chanmin Su and Jian Shi are with the Veeco Instruments Inc. Santa Barbara, CA 93117 USA.

The development of a robust AFM based nanomanipulation system therefore becomes increasingly important. In recent years, extensive work has been done by researchers trying to integrate tele-operation [8][9] into the whole picture. We have developed the augmented reality control system for nanomanipulation [10]. The way they did it is by using a haptic device (Phantom, SensAble Technologies, Inc, Woburn, MA USA) to input the desired position of the AFM cantilever. The coordinate of the joystick will be mapped to the nano-scale space and the position of the joystick will be converted to control voltage and applied to the Piezo actuator. Therefore, the image obtained from the AFM scanning can be used to direct the manipulation while the interaction of the tip and the nano-scale objects can be modeled to give the operator the force feedback. The schematic drawing is shown in Fig. 1.

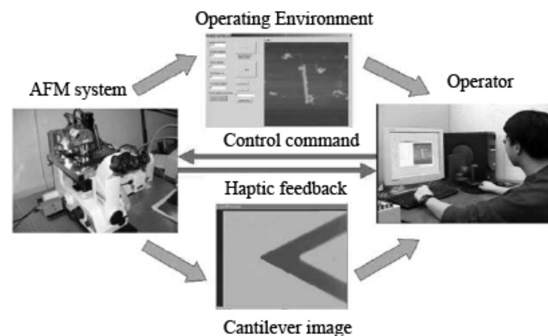

Fig. 1. The augmented reality nanomanipulation system.

The main problem in implementing such a nanomanipulation system lies in the control of the piezoelectric acuator movement. The control problem can be formulated into two categories, the modelling and control of the piezoelectric tube and the overall scheme design and implementation for the whole system. The former has been addressed by researchers [11]. The adaptive controller is developed for compensating the uncertainties in the piezotube actuator. The latter in terms of the control scheme has been lack of attention.

This paper is organized in the following way. In section 2, the problem formulation is discussed by indicating potential control schemes. Then section 3 delineates the control schemes and the problems encountered. By proposing and analyzing the most effecive scheme, section 4 gives out the system performance. Section 5 discusses the results.

II. Problem Formulation

AFM operates by using a cantilever with a sharp tip to move across the sample surface to probe its topography. The main function unit is the piezolelectric tube which actuates the cantilever and the tip both horizontally-the XY scanning direction and vertically-the Z movement direction. When it works, the interaction force between the scanning AFM tip and the sample surface will bend the cantilever. A laser which will be reflected from the back of the cantilever is able to record this deflection by a position sensitive split photodetector (PSD). The Z piezo will move accordingly to keep the tip at a contant distance from or in contact with the sample. The schematic drawing of the working principle of AFM is shown in Fig. 2. Besides the normal scan-imaging task, AFM can perform manipulation as well.

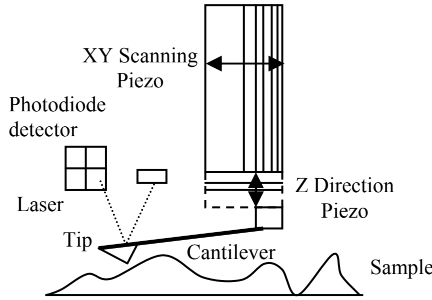

Fig. 2. Schematic drawing of an AFM scanner.

A. Scanning

When doing scanning in either X or Y direction, the AFM control system just inputs a triangle wave voltage (shown in Fig. 3) ranging from -10 to 10 (V); after amplification, the voltage becomes from -110 to 110 (V). This voltage will be applied directly to the piezoelectric transducer which will do the scanning.

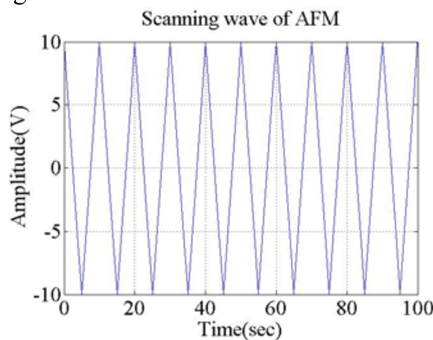

Fig. 3. Scanning wave of an AFM with frequency of 0.1 Hz

The position of the scanning tip can be obtained and feedback to the controller for the close-loop compensation. The output voltage from the AFM controller (-10 to 10) will be corresponding to a scanning region of 100 μm. Shown in Fig. 4 is the control scheme of the AFM scanning and imaging system. The control scheme for doing nanomanipulation will be much more complex and flexible.

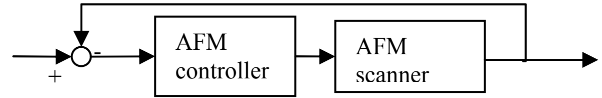

Fig. 4. Control scheme of the scanning AFM system.

B. Manipulation:

When performing nanomanipulation tasks, the AFM tip which is mounted on the Piezo actuator (shown in Fig. 3) will be moved by the specially designed voltage stream rather than a triangular profile. The benefit for this is that we can pattern our own control voltage to achieve a particular task.

The AFM system that we use is Bioscope and the controller is Nanoscope IV (Veeco Instruments Inc, Santa Barbara USA). The Signal Access Module (SAM) can provide the interface between the external input and the AFM system itself shown in Fig. 5. On the basis that the scanner property has been identified, we try to find an effective and effient way to apply the control signal to the scanner so that various criteria can be met. The AFM software provides us an interface where we can define our own input. At the meantime, the signal access module will make the signal feedback and the hardware input channel available for additional modulation.

Fig. 5. The AFM system and the signal access module.

Then the question comes when we have multiple points where the control voltage can be merged into the whole system just as depicted in Figure 5; the voltage can be added right ahead of the AFM scanner (point A in Fig. 6) or before the AFM controller (point B in Fig. 6). Therefore the feasibility and efficiency of each scheme should be assessed whilst the outcome should be compared.

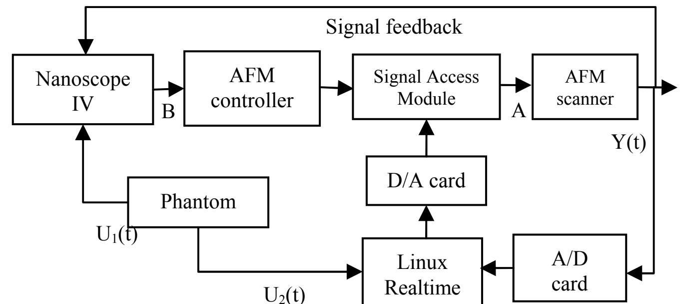

Fig. 6. The Linux feedback control implementation.

The simplest way is to apply the voltage through the software interface (Nanoscope IV). The software provides a macro mechanism which allows developers to compile a

Dynamic-link library (.dll) file and load it when doing manipulation. This integrates the customer program into the whole software. But the overall system response will become very slow in a few hertz frequency due to the software rebuilding process. The external Linux controller is then considered and finally the multiple input control scheme is proposed.

C. System parameter identification

The scanner can be modeled as a second order system with a resonant frequency of f_0 and a Q factor of $1/Q_0$ which results in a damping ration $\zeta = Q_0/2$. Therefore the transfer function of the AFM scanner can be obtained as:

$$G(s) = \frac{\varpi^2}{s^2 + 2\zeta\varpi s + \varpi^2} = \frac{(2\pi * f_0)^2}{s^2 + \frac{(2\pi * f_0)}{Q_0} s + (2\pi * f_0)^2} \quad (1)$$

The PI controller can be identified experimentally. The DC gain of the overall controller is obtained as K_0. In the experiment, we find that when the proportional gain of the controller exceeds K_p, the piezoelectric actuator will become noisy, which means the oscillation of the applied voltage is too high. Hence, the proportional gain should be set as K_p and the integral gain K_0/K_p.

III. SINGLE INPUT CONTROL SCHEMES

A. Input the control signal from point A:

1) Linux mapping

The intuitive way of achieving the goal would be adding the control voltage right in front of the scanner shown in Fig. 7. Firstly, the open-loop method has been tried. Two linear mapping equations (2) are adopted to correlate the input voltage signal with the position of the AFM tip.

$$x_{voltage} = a_1 * X_{position} + b_1$$
$$y_{voltage} = a_2 * Y_{position} + b_2 \quad (2)$$

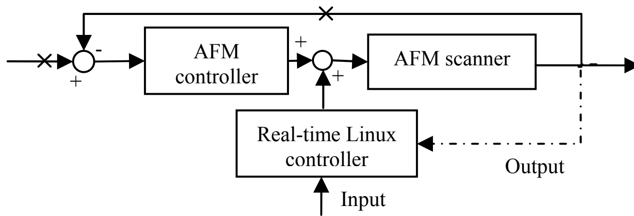

Fig. 7. Open (without dash) and close-loop Real-time Linux control scheme.

Therefore the focus would be finding appropriate parameters (a_1, b_1, a_2 and b_2) for the controller and calibrating them. Here the AFM nanolithography experiment has been done to help calibrating the parameters. We inscribe a horizontal line and a vertical line to calibrate the X and Y respectively shown in Fig. 8. Although the regular manipulation tasks through joystick can be accomplished by this mapping method after a substantial amount of calibration effort, still the lack of sensor feedback will sometimes harm the whole system, especially when the operators impose abrupt motions. Nevertheless, since the control voltage is directly applied to the AFM scanner from the D/A channels by the real-time Linux, the response is quite fast.

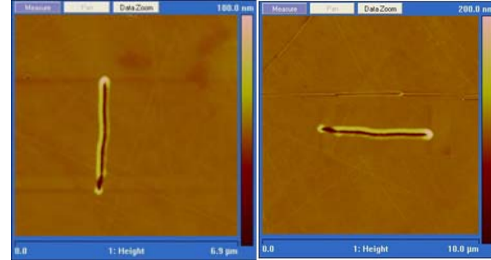

Fig. 8. Nanolithography of a horizontal and vertical line for calibration of x and y mapping parameters.

2) Close-loop Linux controller

A PI controller is designed to replace the original controller and implemented in Linux as indicated by Figure 6. Since by experiment we have identified the parameters of the original controller, they are then adapted to the Linux real-time controller. A typical scanning wave pattern was generated in real time and added to the Linux controller and then applied to the scanner. The RTAI (RealTime Application Interface for Linux) architecture was employed to accomplish the real time control task. The PI controller is working inside the real time module as well as the triangular wave generation process. The triangular signal with peak to peak amplitude of 2 volts is tracked by AFM scanner. A threshold is set for the controller such that a new sample can be generated only after the previous sample has been fully tracked. That is when the difference between consecutive voltage feedbacks is within 0.001 volts.

$$X - X_{previous} <= 0.001V \quad (3)$$

The output from the scanner is observed from the oscillation scope - a scanning wave with a frequency of around 1 Hz shown in Fig. 9.

Fig. 9. Typical scanning wave response and a step response of the real-time control system.

B. Input the control signal from point B:

The external Linux controller is able to accomplish a stable close-loop control system. But the lack of high frequency response is not as desirable. Since we have the original controller which is hardware-based implemented within the AFM system itself, it would be more efficient if we could integrate that into the new setup. We start with the

theoretical basis for this idea.

By observing the whole control scheme, we revisit the signal transformation process of the following. The signal from the PI controller is (shown in Fig. 10A):

$$U'(t) = K_p(U(t) - Y(t)) + K_i \int (U(t) - Y(t))dt \qquad (4)$$

Which is a sum of two signal components $U'_1(t)$ and $U'_2(t)$:

$$U'_1(t) = K_p U(t) + K_i \int U(t)dt \qquad (5)$$

$$U'_2(t) = K_p(-Y(t)) + K_i \int (-Y(t))dt \qquad (6)$$

Therefore we obtain these two components separately from two controllers: the original controller and the external Linux controller shown in Fig. 10B.

Besides, another benefit that we can get from this configuration is that the original controller which has a high response frequency can be utilized.

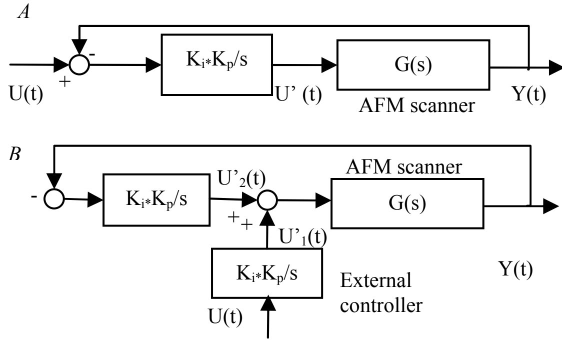

Fig. 10. PI controller with input and output signal.

However, the implementation result shows that there will be saturation in both branches of the control signal. Since the output from the original controller as well as the Linux D/A card (Fig. 6) both have a saturation range from -10 V to 10 V corresponding to the scanning range of 100 µm. The range of the input U(t) without causing the saturation of either branch is around 0.5V shown in Fig. 11 which corresponding to a nanomanipulation range of 5 µm. The result itself is somewhat acceptable. Since most of the time the nanomanipulation operation is concentrated on a small area of sub-micron.

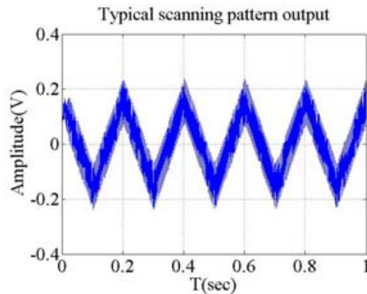

Fig. 11. A small range of input can be tracked without saturation.

We can add a feedback loop to the external controller to the system. The whole system will become a double loop system shown in Fig. 12. The idea is by introducing an outer loop, the desired position can be controlled by a slower loop implemented in the Linux real time system; while the inner loop which has a faster response can be used to direct the scanner tip to the desired position in high frequency.

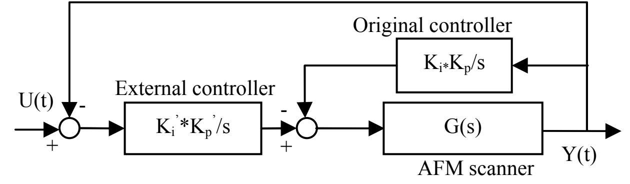

Fig. 12. Additional input to the AFM controller to overcome the saturation.

The new system can be studied by consider the inner loop as a new plant G'(s).

$$G'(s) = \frac{G(s)}{1 + GH(s)} = \frac{\varpi^2 s}{s^3 + 2\zeta\varpi s^2 + \varpi^2 s + K_i K_p \omega^2} \qquad (7)$$

where H(s) is the original controller transfer function. By using the transform, a new external controller can be designed according to the new transfer function.

Still the saturation problem will cause the feedback compensation fail, although the input signal tracking range is improved compared to the previous setup.

IV. Multiple Input Control Scheme

By observing the simulation, we will be able to tell that the saturation is caused by the input to the original controller. Since the input to the AFM original controller is supposed to be the difference $U_{err1}(t)$ between the desired position and the feedback position from the scanner; it will be in a quite small range shown in Fig. 13 left.

$$U_{err1}(t) = U(t) - Y(t) \qquad (8)$$

After we change the control scheme by introducing the external controller which has the input of the desired position, the feedback from the scanner becomes the only input to the original controller $U_{err2}(t)$, which makes it very large (shown in Fig. 13 right).

$$U_{err2}(t) = -Y(t) \qquad (9)$$

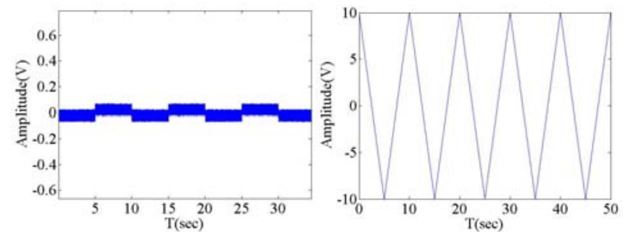

Fig. 13. The input to the AFM controller left: the original setup(A in Fig. 9); right: the designed setup (B in Fig. 9).

The inputs to the system are both the scanning wave shown in Figure 1. Therefore the saturation problem can be overcome by introducing an additional input to the original controller. The aim is to bring down the input by compensation and then avoid saturation. The control scheme

is shown in Fig. 14.

This control scheme can be analyzed in two different situations. Firstly, we assume that the input signals to both the original controller and the external controller are the same $U_1(t) = U_2(t) = U(t)$.

Therefore the signal coming from them will be:

$$U_{or}(t) = K_p(U_1(t) - Y(t)) + K_i \int_0^t (U_1(t) - Y(t))dt \quad (10)$$

$$U_{ex}(t) = K_p(U_2(t) - Y(t)) + K_i \int_0^t (U_2(t) - Y(t))dt \quad (11)$$

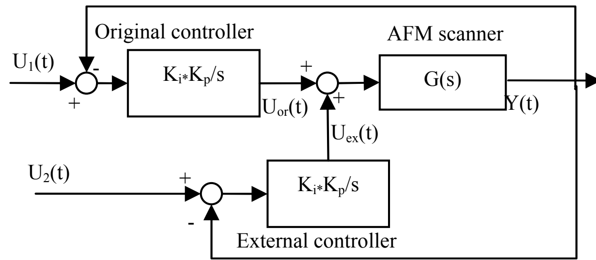

Fig. 14. Additional input to the AFM controller to over come the saturation.

Since the input signal is the same, then we have $U_{or}(t) = U_{ex}(t)$. In this case, the system can be regarded as a single controller scheme where the controller has proportional and integral gain doubled as compared to the original controller.

The step response to the above configuration is shown in Fig.15. Compare to the original setup, the step response is much better in shape.

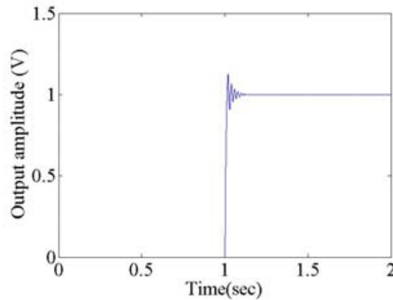

Fig. 15. Step response of the new configuration.

Secondly, the signal inputs to both the controllers are different with $U_1(t) \neq U_2(t)$. This means that at a given time t there is an offset between $U_1(t)$ and $U_2(t)$. This situation could be caused by the different sampling frequency of the two controller branches. Although the signal source is the same, a short period of time delay will result in an offset between the two signals. From this point of view, the offset can be assumed to be quite small.

A. Step response

Assume for now that $U_1(t) < U_2(t)$. The situation is simulated by taking the $U_1(t)$ as a step input while $U_2(t)$ is a step input with amplitude 1.2. The signal outputs from both controllers are in the form of equation (10) and equation (11). They are not equal obviously with $U_{or}(t) < U_{ex}(t)$. From time zero to t_1 we have the following situation:

$$U_{ex}(t) > 0 \quad U_{or}(t) > 0 \quad (12)$$

The two controllers are working together just like the previous situation when $U_1(t) = U_2(t)$. They bring the output $Y(t)$ to the proximity of the input $U(t)$ which shows up in Fig. 16 as the end period of t_1.

A critical point is reached when the feedback signal $Y(t)$ is equal the smaller input which in this case is $U_1(t)$. This will make $U_{or}(t)$ cross the zero line to the negative region.

Another critical point is when the feedback signal $Y(t)$ reaches the following:

$$Y(t) = \frac{U_1(t) + U_2(t)}{2} \quad (13)$$

This time is set as t_1. It has the following characteristics:

$$U_{or}(t) < 0 \quad U_{ex}(t) > 0 \quad (14)$$

$$U_{or}(t) + U_{ex}(t) = \frac{U_1(t) + U_2(t)}{2} \quad (15)$$

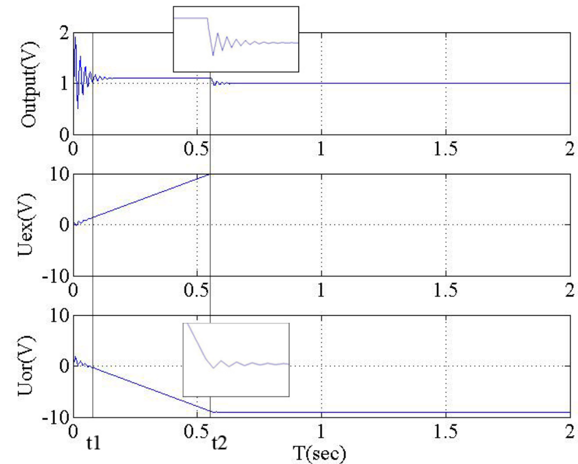

Fig. 16. Step response of the new configuration with two different input values, one is the step input and the other is 1.2 times in amplitude of the step input, above: the output signal from the scanner, middle: the signal output from the external controller (saturated), bottome: the signal output from the original controller(unsaturated).

From t_1 until t_2 these characteristic equations (13), (14) and (15) holds and we call this period a temporarily stable time. The output signals from the controllers are increasing since both have constant error inputs:

$$U_{err1}(t) = U_1(t) - \frac{U_1(t) + U_2(t)}{2} = \frac{U_1(t) - U_2(t)}{2} \quad (16)$$

$$U_{err2}(t) = U_2(t) - \frac{U_1(t) + U_2(t)}{2} = \frac{U_2(t) - U_1(t)}{2} \quad (17)$$

The proportional terms remain the same while the integral errors will keep adding up. The last critical point t_2 is reached when one of the controller outputs get saturated, which in this case is $U_{ex}(t)$. From this time on, the original controller which is active will adjust the output to overcome

a constant disturbance $U_{ex}(t_2)$ which is equal 10. The stabling process is shown in the inset of Fig. 16.

Finally, when the whole system is stable, the output from the scanner is tracking the final voltage from the original controller. The saturation problem is overcome since one of the controllers can be at an active state while the other in saturation. We want to stay within the first stage if we want a higher response frequency, which will give us the settling time which is around 0.025s corresponding to a frequency of 40 Hz.

B. Continuous input

We then input a continuous signal rather than the step input above, but there exists a sampling frequency difference which is the real case with the current system since the signal to the original controller is merged to the system from the internal control software and directly applied to the scanner, while for the external controller the voltage is applied through the D/A converter.

As in the continuous input, the system will always perform at the first stage illustrated above from time zero till time t_1. With most systems the sampling frequency will be much larger than 40 Hz; hence the time it takes for new sample to arrive is shorter than t_1 which is around 0.025 seconds. When new samples arrive, both controllers will work together to obtain a new equilibrium. Therefore, overall system will track $\frac{U_1(t)+U_2(t)}{2}$ at all times. Besides, with a high enough sampling frequency the equation below approximately holds.

$$U_1(t) = U_2(t) = \frac{U_1(t)+U_2(t)}{2} \quad (18)$$

Here the scanning pattern is used as input to both the external and the original controller with sampling frequency at 10 Hz and 20 Hz respectively. The result shows that the saturation problem will not be a factor anymore, since most of the time there will be one controller which is not saturated as illustrated in Fig. 17. But there will be a subtly short period when both of them are saturated indicated by the grey line. There will be a small kink in those time periods as magnified in the inset. When looked further, this small kink can be eliminated by increasing the sampling frequency. Since we are using only 10 and 20 Hz as examples, when the frequency is four folds of those, there will be no saturation and no abnormality anymore.

V. Conclusion

In the paper, several control schemes have been studied in the AFM nanomanipulation platform through using a specially designed signal access module. An external controller has been implemented in the Linux real time framework. With the single input system, it works well but has the low frequency problem; we can only do manipulation at a few Hz. Then we integrated the original controller to the system for a fast response, but there comes the saturation problem causing the nanomanipulation system only working in 5 micron range. The saturation problem has been overcome by an additional input from both the original AFM controller and the external controller. It is found out that at any given time at least one of the controllers will be able to stay active and make the system stable. This multiple input single input control not only overcome the saturation problem but also has a high frequency response which is around 40 Hz. When we perform manipulation tasks, this frequency is high enough for the human hand operating the haptic device.

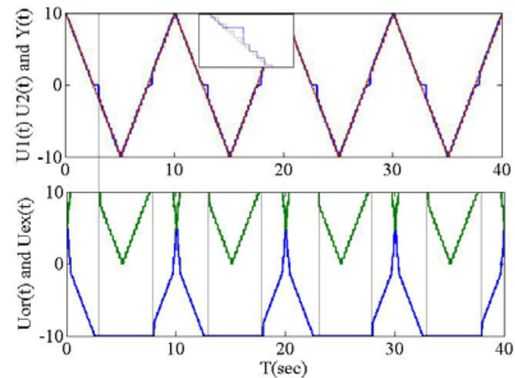

Fig. 17. The continuous scanning pattern tracking (above) with the output signal from both the controllers (bottom).

References

[1] C. Martin, G. Rius, X. Borrise and F. P. Murano, "Nanolithography on thin layers of PMMA using atomic force microscopy," *Nanotechnology*, vol. 16, pp. 1016-1022, 2005.

[2] G.Li, N. Xi, H. Chen, A. Saeed and M. Yu, "Assembly of nanostructure using AFM based nanomanipulation system," *IEEE Int. Conf. on Robotics and Automation*., New Orleans, LA, Aprial 2004.

[3] A. A. G. Requicha et. al, "Nanorobotic assembly of two-dimensional structures," *IEEE Int. Conf. Robotics and Automation*, Leuven, Belgium, May 1998, pp. 3368–3374.

[4] J. Zhang, G. Li, N. Xi, "Modeling and control of active end effector for the AFM based nano robotic manipulators," *Int. Conf. on Robotics and Automation,* Bacelona, Spain, 2005.

[5] G. Y. Li, N. Xi, and M. Yu, "Calibration of afm based nanomanipulation system," in *Proc. IEEE Int. Conf. Robotics and Automation*, New Orleans, LA, Apr.–May 2004.

[6] M. Guthold, M. R. Falvo, W. G. Matthews, S. Washburn, S. Paulson, and D. A. Erie, "Controlled manipulation of molecular samples with the nanomanipulator," *IEEE/ASME Trans. Mechatron.*, vol. 5, pp. 189–198, June 2000.

[7] C. Thelander and L. Samuelson, "AFM manipulation of carbon nanotubes: realization of ultra-fine nanelectrodes," *Nanotechnology*, vol. 13 pp.108-113 2002.

[8] M. Sitti, B. Aruk, H. Shintani and H. Hashimoto, "Development of a scaled teleoperation system for nano scale interaction and manipulation," *Int. Conf. on Robotics and Automation*, Seoul, Korea, May 2001.

[9] B. Aruk, H. Hashimoto, and M. Sitti, "Man-machine interface for micro/nano manipulation with afm probe," *IEEE Int. Conf Nanotechnology*, Maui, HI, Oct. 2001, pp. 151–156.

[10] G. Li, N. Xi, M. Yu and W. Fung, "Development of augmented reality system for AFM based nanomanipulation," *IEEE Trans. On Mechatronics*, vol. 9, no. 2 pp.358-366, 2004.

[11] K. Rifai, O. Rifai and K. Toumi, "Modeling and control of AFM-based nano-manipulation systems," *Int. Conf. on Robotics and Automation, Barcelona*, Spain, 2005.